Honeycomb-Structured Porous Films from Polypyrrole-Containing Block Copolymers Prepared via RAFT Polymerization as a Scaffold for Cell Growth

Danelle Beattie,[†] Kok Hou Wong,[†] Charles Williams,[‡] Laura A. Poole-Warren,[‡] Thomas P. Davis,[†] Christopher Barner-Kowollik,[†] and Martina H. Stenzel*[,†]

Centre for Advanced Macromolecular Design (CAMD), School of Chemical Engineering and Industrial Chemistry, The University of New South Wales, Sydney, NSW 2052, Australia, and Graduate School of Biomedical Engineering, The University of New South Wales, Sydney, NSW 2052, Australia

Received November 9, 2005; Revised Manuscript Received February 14, 2006

Honeycomb-structured porous films were prepared using customized amphiphilic block copolymers, synthesized by RAFT polymerization. Pyrrole was templated along an amphiphilic block copolymer, composed of polystyrene and poly(acrylic acid). Subsequent oxidation of pyrrol to polypyrrole, resulted in the formation of a soluble polypyrrole-containing polymer. Gel permeation chromatography and dynamic light scattering studies confirmed the solubility of the resulting customized amphiphilic block copolymer, in both water and organic solvent, forming either micelles or inverse aggregates. Porous films with a hexagonal array of micron-sized pores were generated with the polymer, using the breath figures templating technique. The resulting films were found to be non-cytotoxic and hence suitable as scaffolds for tissue engineering. Initial fibroblast cell culture studies on these scaffolds demonstrated a dependency of cell attachment on the pore size of scaffolds.

Introduction

Electrically conducting polymers are proposed as having potential for applications such as batteries, sensors, antistatic coatings, and microelectronic devices. However, more recently, the potential use of these polymers in biological systems has raised considerable interest. The stimulation of biological systems with electrical currents is known to be beneficial for the growth of cells.[1] Typical conducting polymers, utilized to interact with amino acids, proteins, enzymes, or living cells, are polyanilines, polythiophenes, and polypyrroles. In vivo studies have concluded that polypyrrole is not cytotoxic and is biocompatible at moderate quantity. It can be fabricated into conducting conduits that support the regeneration of damaged peripheral nerves in rats.[2−4] It has also been shown that electrical stimulation of PC-12 cells (neuron-like cells) on polypyrrole substrates resulted in a twofold amplification of neurite outgrowth in comparison to controls not subjected to electrical stimulation.[2,3] Cell adhesion is strongly dependent on the surface chemistry of the substrates, such as hydrophobicity or surface charge[5] and topography.[6] Polypyrrole, in its intrinsic state, is rather brittle and is an insulating material with a nondegenerate ground state and a band gap (E_g) of 3.2 eV between valence and conduction bands.[7] The conductivity of intrinsic polypyrrole, however, can be transformed from insulating ($\sigma_{dc} \leq 1 \times 10^{-7}$ S cm^{-1}) to metallic ($\sigma_{dc} \geq 1 \times 10^{2}$ S cm^{-1}) through the process of oxidative doping.[8] Dopants commonly employed include small anions,[9,10] polymeric anions,[3,11,12] buffer salts or ionic liquids,[13] and biologically active anions such as adenosine triphosphate, hyaluronic acid, heparin, antibodies, enzymes, and even living cells.[1] Dopants not only alter the conductivity of polypyrrole but also increase the solubility of the otherwise insoluble polypyrrole. Solubility in water or in organic solvents is important and is a prerequisite for certain processing techniques, such as the preparation of conductive coatings[14] that involves the evaporation of solvent while the polymers organize in a certain order. Preparation of polypyrrole is typically facile and involves oxidative polymerization either chemically or electrochemically, with a dopant anion being incorporated into the polymer chain. Polymerization conditions not only determine the polymer composition but also influence the structure of the polymer, from the molecular level to the macroscopic level.[15]

The aim of this study is the synthesis of polypyrrole-containing polymers that can easily be processed into porous films suitable for tissue engineering. While polypyrrole is usually insoluble, we propose the templating of pyrrole along a poly(acrylic acid) chain resulting in water-soluble polymers. Poly(acrylic acid) not only enhances the solubility of the polymer but also acts as a dopant.[12] Pyrrole coordinates with acid groups such as poly(acrylic acid)s via hydrogen bonds. The subsequent polymerization of the adsorbed pyrrole should result in the polypyrrole aligned with the acrylic acid segments. This templating polymerization leads to oriented growth of polypyrrole[12] and subsequently into water-soluble conducting polymers. The attachment of hydrophobic sequences results in the formation of amphiphilic structures, presenting good solubility both in aqueous solutions as well as in organic solvents. (Scheme 1)

Being based on an amphiphilic block copolymer structure, the polymers synthesized can undergo self-assembly into micellar and inverse micellar structures, thus being suitable to be processed into coatings and films. To demonstrate the possibility of processing these polymers from organic solvents into a porous polymer scaffold, we employ the breath figure technique. This technique allows the formation of conducting regular porous honeycomb-structured films prepared via breath figures.[16−18] Some preliminary results on the usage of these

* Corresponding author. E-mail: camd@unsw.edu.au.
[†] Centre for Advanced Macromolecular Design.
[‡] Graduate School of Biomedical Engineering.

10.1021/bm050858m CCC: $33.50
Published on Web 03/25/2006

Scheme 1: Synthesis of PS−PAA Block Copolymers via RAFT Polymerization Followed by the Adsorption of Pyrrole onto the PAA Block and the Subsequent Oxidation to Polypyrrole

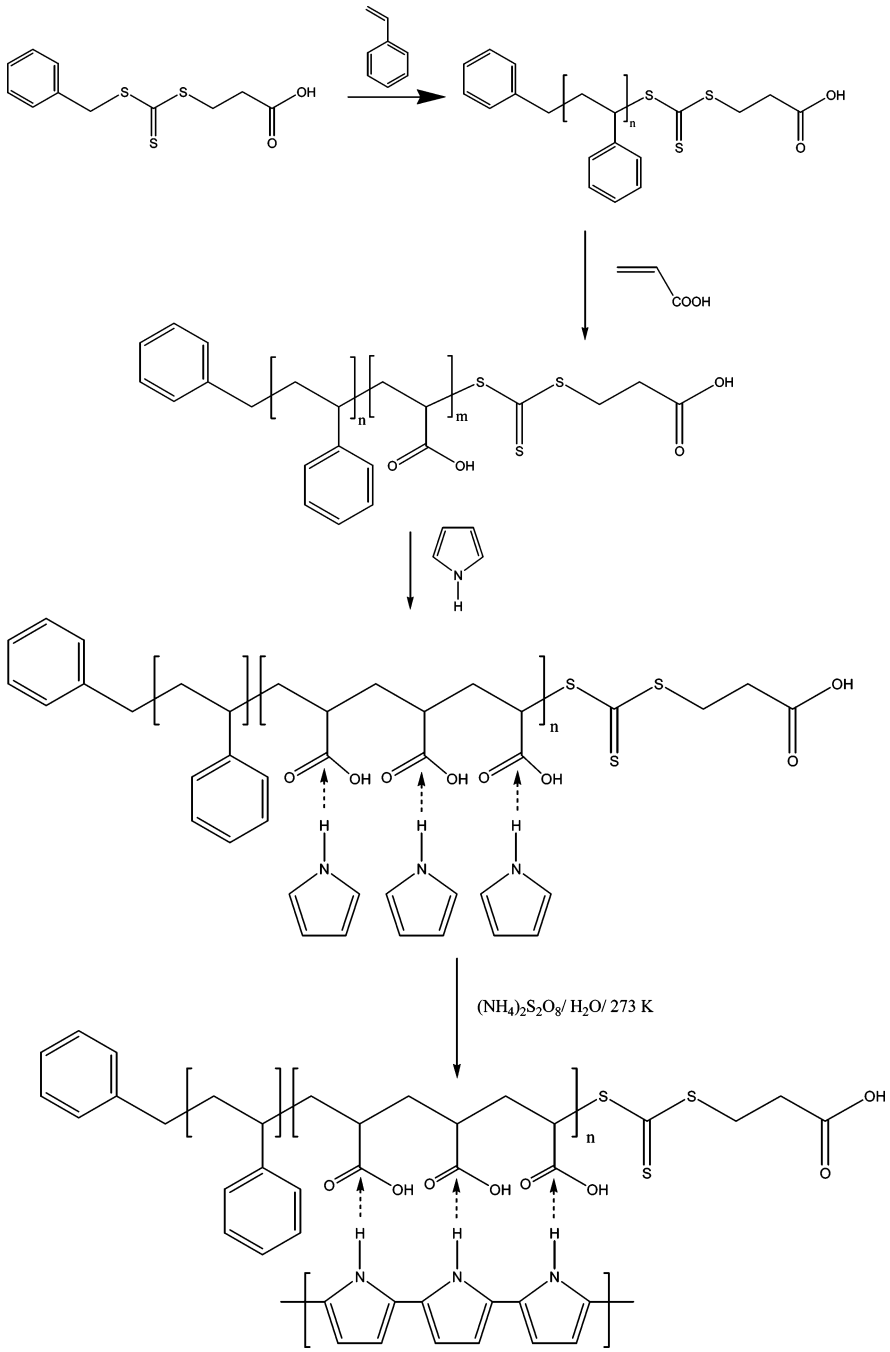

honeycomb-structured porous films as a surface for tissue engineering will be presented.

RAFT polymerization[19−21] is a versatile way to prepare amphiphilic block copolymers,[22−24] since functional groups such as carboxylic acids do not interfere with the living behavior of the polymerization. The polymerization can even be easily carried out in aqueous environment[25] and has been shown to be suitable for the controlled polymerization of acrylic acid.[26−28]

Experimental Section

Materials. 2,2′-Azobis(2-cyanopropane) (AIBN, Aldrich, 98%) was purified and used as the thermal initiator in all polymerizations involving acrylic acid. Acrylic acid (AA, Aldrich, 99%) was distilled and stored below 4 °C, while styrene (Aldrich, 99%) was deinhibited using an alumina column. The RAFT agent used in the polymerization of both AA and styrene, 3-benzylsulfanylthiocarbonylsulfanyl propionic acid, was prepared according to the procedure described elsewhere.[29] *N*,*N*-Dimethylacetamide (DMAc, Aldrich, 99.9%) was used as the solvent, without further purification. Pyrrole (Py, Aldrich, 98%) was distilled under vacuum, prior to polymerization, and was initiated by the addition of ammonium persulfate (APS, Aldrich, 98%).

Polymerization. Poly(acrylic acid) was prepared by dissolving monomer (4.32 g), AIBN (0.0019 g), and benzylsulfanylthiocarbonylsulfanyl propionic acid (0.0326 g) in DMAc (25.9558 g). The reactant solution was poured into a 100 mL vacuum flask and degassed via several freeze−thaw−evacuate cycles. The contents were then transferred into sample bottles, purged with nitrogen, and sealed with rubber septa, before placing into an isothermal water bath at 60 °C to polymerize. Sample bottles were subsequently removed at regular time intervals and quenched, via submergence in a beaker of ice cold water.

Conversions were determined gravimetrically following evaporation of monomer and solvent.

Polystyrene−poly(acrylic acid) block copolymers (PS−PAA) were synthesized from polystyrene macroRAFT agent using benzylsulfanylthiocarbonylsulfanyl propionic acid.[29] PS macroRAFT agent (M_n = 25 000 g mol^{-1}, 2.70 g), AA (4.13 g), and AIBN (0.0018 g) were weighed directly into a 200 mL vacuum flask and dissolved in DMAc (25.96 g) using a magnetic stirrer. The reaction mixtures was degassed via several freeze−thaw−evacuate cycles, transferred into bottles, sealed under vacuum, and purged with nitrogen. The bottles were then placed in an isothermal oil bath at 60 °C to polymerize, and at regular time intervals were removed and quenched. Conversions were determined gravimetrically following evaporation of monomer and solvent.

Pyrrole monomer (0.0485 g) was weighed into six separate glass sample tubes containing PAA (0.1430 g). Distilled water (3.00 g) was added to each sample tube, and the contents were thoroughly mixed, using a magnetic stirrer, for 3 days. Different quantities of APS (0.0452 g, 0.0318 g, 0.0238 g, 0.0213 g, 0.0167 g, 0.0132 g) were then dissolved in distilled water (2.00 g) to achieve [Py]/[APS] = 3.5, 6.1, 6.9, 7.4, 10, and 12, respectively. APS(aq) was then added dropwise to each of the PAA/Py stirred solutions, over a period of 4−5 min. The polymerization was carried out for 1 h at room temperature before being quenched by the addition of MeOH (2 mL).

Samples for the polymerization of pyrrole involving PS−PAA block copolymer were prepared by dissolving the polymer at the appropriate concentration in *N,N*-dimethylacetamide and subsequently dialyzing against water using tubular membranes. Stoichiometric amounts of pyrrole were added, and the polymerization was carried out accordingly.

Analysis. *Fourier Transformed Near-Infrared (FT-NIR) Spectroscopy.* Solutions were degassed by purging nitrogen for 1 h. Monomer conversions were determined via on-line Fourier transform near-infrared (FT-NIR) spectroscopy by monitoring the decrease of the intensity of the vinylic stretching overtone of the monomer at $\nu = 6150$ cm^{-1}. The FT-NIR measurements were performed using a Bruker IFS66\S Fourier transform spectrometer equipped with a tungsten halogen lamp, a CaF_2 beam splitter, and a liquid nitrogen cooled InSb detector. Each spectrum in the spectral region of 8000−4000 cm^{-1} was calculated from the coadded interferograms of twelve scans with a resolution of 4 cm^{-1}. For conversion determination, a linear baseline was selected between 6260 and 6100 cm^{-1}. The integrated absorbance between these two points was subsequently used to calculate the monomer to polymer conversion via Beer−Lambert's law. It should be noted that other integration methods such as using only the variation of the peak height at 6150 cm^{-1} have been tested and yield identical results.

Size Exclusion Chromatography (SEC). Molecular weight distributions of polymers were determined by size exclusion chromatography (SEC) using a Shimadzu modular system, comprising an autoinjector, a Polymer Laboratories 5.0 μm bead-size guard column (50 × 7.5 mm), followed by three linear PL columns (10^5, 10^4, and 10^3 Å) and a differential refractive index detector. The eluent was *N,N*-dimethylacetamide (0.5% LiBr) at 40 °C with a flow rate of 1 mL·min^{-1}. The system was calibrated using narrow polystyrene standards ranging from 500 to 10^6 g·mol^{-1}.

Conductance Measurements. Direct conductance measurements were performed using a DT83 digital multimeter, with an operating range between 5×10^{-3} and $5 \times 10^{-7}\Omega^{-1}$ and reported accuracy of ±0.5%. For all conductivity measurements, A/C distance was maintained at a constant 15 mm.

Thermal Gravimetric Analysis (TGA). Thermal decomposition properties of polymers were recorded using a Perkin-Elmer themogravimetric analyzer (Pyris 1 TGA). Analyses were conducted over the temperature range 30−500 °C with a programmed temperature increment of 30 °C/min.

Differential Scanning Calorimetery (DSC). Perkin-Elmer differential scanning calorimeter (DSC 7) and thermal analysis controller (TAC 71DX) were used in conjunction to measure glass transition temperatures. Samples were analyzed in 50 μL pans, over the temperature range 35−200 °C with scanning rate of 30 °C/min.

Dynamic Light Scattering (DLS). DLS experiments were performed on a Brookhaven Zeta Plus laser light scattering spectrometer. All measurements were recorded at 25 °C, using an angle of 90° and wavelength of 678.0 nm. ZetaPals particle sizing software (version 3.57) was used to obtain the distributions of hydrodynamic diameter $f(D_h)$ for each set of measurements.

Transmission electron microscopy (TEM). The TEM micrographs were obtained using a Hitachi H7000 transmission electron microscope. The samples were prepared by casting a low-concentration solution of water (1 g L^{-1}) onto a copper grid. The solvent was allowed to evaporate at room temperature. The samples were stained with OsO_4.

Preparation of Honeycomb-Structured Porous Films.[30] Casting of polymer complexes was carried out at ambient temperatures, in a humidified compartment of an enclosed Perspex box. Relative humidity levels between 70% and 79% were maintained via a constant influx of moist air through dual connector hoses located at the top and side of the casting chamber, and buffered by an adjacent saline reservoir containing dissolved Na_2CO_3 salts. A vacuum pump, capable of supplying a maximum flow rate of 70 L/min, was used to pump air through a two-stage water pass (~3 L) and deliver a constant moist airstream through both connector hoses. Polymer in carbon disulfide (10 mg mL^{-1}) was deposited (volumes: (i) 10 μL; (ii) 0.5 mL) onto to (i) glass slides or (ii) glass Petri dish, inside the casting chamber, using a (i) micropipet or (ii) disposable plastic dropper. The top connector hose inserted into an elongated slot immediately above the casting area could be moved back and forth to achieve some degree of control over the localized flow of moist air past the slides and the subsequent rate of solvent volatilization. A more detailed description of the techniques is available elsewhere.[16,30]

Cytotoxicity Testing. Samples for cytotoxicity testing were prepared by casting a polymer solution from carbon disulfide or methylene chloride according to the techniques described above into a Petri dish with an area of 22 cm^2. The dry samples were immersed in a 0.1% solution of Deacon 90 in water and then washed with water. The samples were sterilized using Co^{60} over 4 h.

Cytotoxicity of polymer films prepared was determined using a cell growth inhibition assay with L929 mouse fibroblasts. Extraction of polymer films was carried out by incubation in complete media (Eagle's Minimum Essential Medium + 10% fetal bovine serum) at 37 °C for 24 ± 2 h at a ratio of 0.2 μL of medium per cm^2 of polymer film.

Extracts from the films were applied to a subconfluent monolayer of cells seeded 24 h earlier. The cells were then incubated for 48 ± 3 h at 37 °C. After this time, the cells were trypsinized, stained with propidium iodide (PI), and subsequently analyzed for total live cell counts with live/dead assay using a fluorescently activated cell sorter (FACS). Fluorescent green beads (10 μm diameter) were added to all samples and were used as an internal counting reference. Inhibition data were obtained by comparing the number of live cell counts of experiment (PS−PPy films) to the control (tissue culture plastic) of LIVE/LATEX/DEAD groups, from the dot-plot outputs, of flow cytometry in WinMDI program.

Cell Growth Experiments. Cell adhesion and growth on porous polymer films was assessed by fluorescent microscopy. L929 mouse fibroblasts with a cell seeding density of 9500 cell per cm^2 of polymer film were used.

To assess cell attachment potential, 1.4 mL of cells with a concentration of 50 000 cell/mL of medium was introduced onto polymer film samples cast in 30-mm-diameter Petri dishes and subsequently incubated at 37 °C for 3 h, before an addition of 350 μL of the fluorescent stains dimethyloxardicarbocyanine iodide/propidium iodide (DiOC2/PI) (5:1 v/v). Petri dishes were further incubated at 37 °C for 30 min for stain uptake, rinsed in Dulbecco's phosphate buffered saline (DPBS), and resubmerged in DPBS for microscopy analysis. Cell numbers were assessed as an indication of initial adhesion using

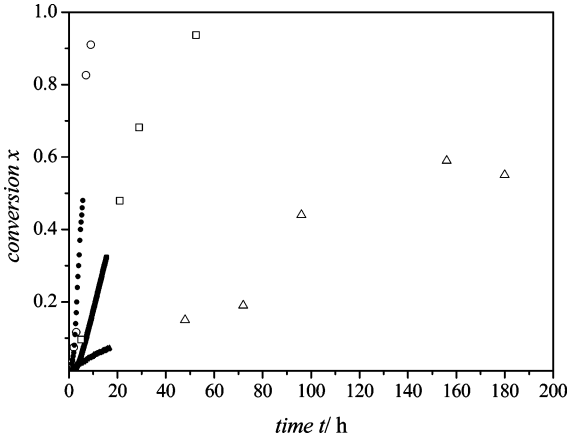

Figure 1. Pseudo-first-order kinetic plot of the polymerization of acrylic acid AA at 60 °C in *N,N*-dimethylacetamide in the presence of the RAFT agent **I** (circle) and polystyrene macroRAFT agent with molecular weights of 6000 (square) and 41 000 g mol^{-1} (triangle). $[AA]_0 = 2.36$ mol·L^{-1}; $[AIBN]_0 = 4.2 \times 10^{-4}$ mol·L^{-1}; $[RAFT] = 4.2 \times 10^{-3}$ mol·L^{-1}. Conversion was obtained via gravimetry (open symbols) and FT-NIR (closed symbols).

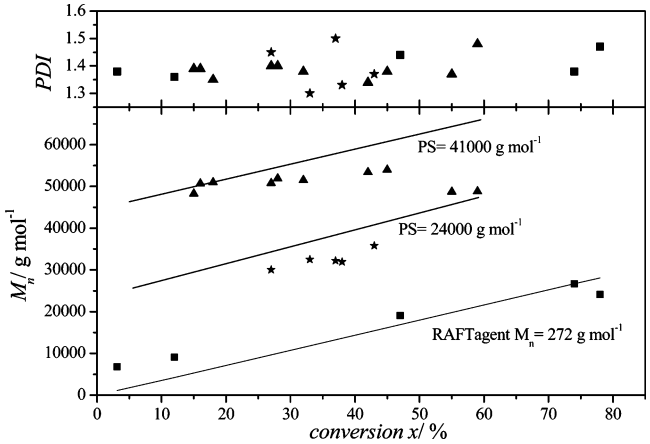

Figure 2. Evolution of M_n and polydispersity index PDI vs conversion x as obtained by SEC of the polymerization of acrylic acid at 60 °C in *N,N*-dimethylacetamide in the presence of the RAFT agent **I** and polystyrene macroRAFT agent of varying molecular weights. $[AA]_0 = 2.36$ mol·L^{-1}; $[AIBN]_0 = 4.2 \times 10^{-4}$ mol·L^{-1}; $[RAFT] = 4.2 \times 10^{-3}$ mol·L^{-1}. The straight line indicates the theoretical molecular weight development calculated from conversion according to M_n (theo) = [M]/[RAFT] $\times$ x $\times$ M_M + M_n (macroRAFT) with [M] and [RAFT] representing the concentrations of the monomer and the thiocarbonyl thio group, respectively; x is the monomer conversion; M_M is the molecular weight of the monomer.

fluorescent microscopy before DPBS removal and an addition of medium to reincubate for further cell growth.

To assess cell growth potential, further incubation of the above at 37 °C for up to 36 h was allowed, treated with DiOC2/PI, as mentioned, and investigated for cell quantity at regular intervals, using fluorescent microscopy analysis.

Results and Discussion

Synthesis of Polystyrene-*block*-Poly(acrylic acid) PS-*b*-PAA. Polystyrene-*block*-poly(acrylic acid) was prepared in the presence of a trithiocarbonate-based RAFT agent. The selected RAFT agent, benzylsulfanylthiocarbonylsulfanyl propionic acid, is known to be non-cytotoxic,[24] and the RAFT polymerization in the presence of trithiocarbonates reportedly proceeds without any apparent retardation.[31] Poly(acrylic acid) was successfully prepared using trithiocarbonate-based RAFT agent.[28] However, earlier research, conducted on the synthesis of acrylic acid using the RAFT polymerization process, has indicated that the polymerization is sensitive to a number of conditions including the nature and concentration of the employed transfer agent and initiator, as well as the solvent used.[26,28] In this work, we used *N,N*-dimethylacetamide as solvent, since it is suitable for both acrylic acid and the polystyrene macroRAFT agent. A range of polystyrene macroRAFT agents varying in molecular weights were used for chain extension with acrylic acid. The length of the polystyrene block seems to have a significant influence on the rate of polymerization of acrylic acid (Figure 1). Gravimetric conversion determinations, as well as FT-NIR experiments, confirm the retardation of the rate of polymerization with increasing polystyrene block length (Figure 1). Since the electronic structure of the RAFT groups does not change with the size of the macroRAFT agent, the retardation observed can only be attributed to an altered solution environment. Increased viscosity, caused by an increased molecular weight, can decrease the initiator efficiency, consequently inflicting a retardation of the polymerization rate.[32] A decreased accessibility of the thiocarbonylthio endgroup can also be considered as a potential source for the rate inhibition. With increasing length of the first block, the endgroup is more and more buried within the chain. At this stage, we can only speculate about the origin of this retardation. It has to be noted that an opposite/contradicting behavior has been observed with the rate of polymerization increasing when the viscosity is increased.[33]

The living behavior of the polymerization was confirmed by the linear molecular weight evolution with conversion. The measured values deviate slightly from the expected molecular weight, which can be attributed to the polystyrene calibration of the SEC (Figure 2). However, the poly(acrylic acid) seems to undergo a slight hybrid behavior, which is usually caused by a slow initial transfer to the RAFT agent and can be identified by a higher molecular weight than expected at low conversions. The molecular weight obtained at high conversion is, in contrast, slightly lower than predicted. This can be derived by the SEC calibration and also to chain transfer occurring to the polymer that has been observed earlier in the RAFT polymerization of acrylic acid.[28] However, the polydispersity index remains constantly below 1.4, and broadening of the distribution is absent.

Polymerization of Pyrrole Templated on Acrylic Acid. The poor solubility of polyprrole is supposed to be derived not only from the weak interactions of polypyrrol with the solvent but also from the formation of cross-links in the 2,3-position.[34] The doping with bulky acidic groups or the introduction of functional groups in the 3-position of pyrrol limits the contact between the polymer chains.[35] The interaction of pyrrole with acidic groups results in a templating effect, which ensures the alignment of polypyrrole.

The chemical oxidation to polypyrrole was carried out in aqueous solution in the presence and absence of poly(acrylic acid) using a range of ammonium persulfate APS $[NH_4]_2SO_5$ concentrations. Freshly distilled pyrrole, water, and in some cases poly(acrylic acid) were combined with APS added instantly. The oxidative polymerization was accompanied by a visible change in color. An initially colorless solution briefly turned green and later dark green, indicating the formation of dimers and oligomers. Depending on the concentrations of pyrrole and oxidant used, the precipitation of a dark black solid was observed, indicating the presence of cross-linked polycationic polypyrrole. In fact, polypyrrole doped with poly(acrylic acid) was found to have a rather limited solubility, which may

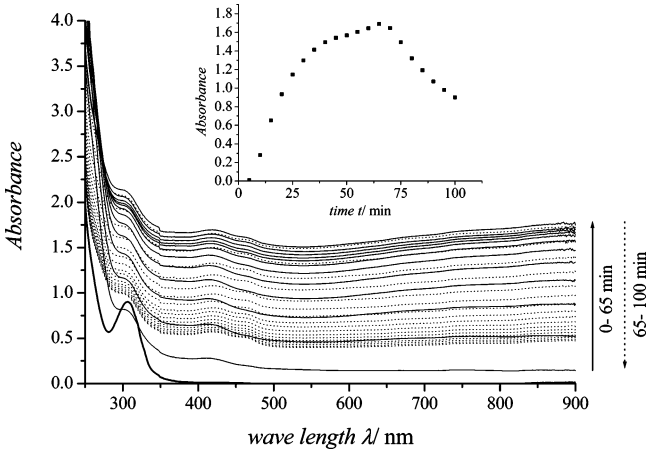

Figure 3. UV−vis scanning kinetics experiment recorded every 5 min of the reaction of pyrrole (1.4×10^{-1} mol·L^{-1}) in water templated on poly(acrylic acid) ($M_n = 32\,000$ g mol^{-1}), oxidized with 1.4×10^{-2} mol·L^{-1} APS. The spectra were recorded after dilution to 2.8×10^{-3} mol·L^{-1} pyrrole. The inserted figure represents the absorbance as measured at a wavelength of 440 nm.

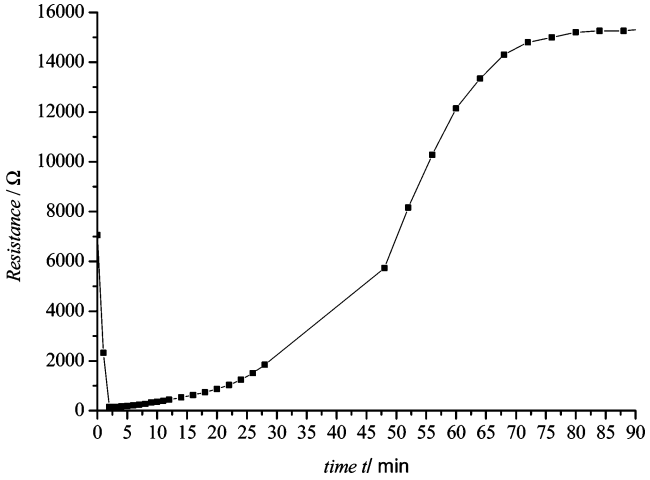

Figure 4. Conductivity measurements (as expressed in resistance) of the solution during the reaction of pyrrole (1.4×10^{-1} mol·L^{-1}) in water templated on poly(acrylic acid) ($M_n = 32\,000$ g mol^{-1}), oxidized with 1.4×10^{-2} mol·L^{-1} APS. The distance of the electrodes was 15 mm.

be indicative of an ineffectual templating. As a consequence, pyrrole was stirred with acrylic acid for an extended period of time (3 days) prior to the addition of ammonium persulfate to allow the complete interaction between carboxy groups and pyrrole. It was found that the solubility of polyprrole could be enhanced by prolonging the time pyrrole and poly(acrylic acid) were allowed to mix prior to the addition of APS. The reaction was monitored by measuring the resistance of the solution and the UV−vis spectra. Samples of the original solution were diluted to a suitable concentration for UV spectroscopy after certain time intervals. Initially, only an adsorption at 306 nm is visible corresponding to the $\pi-\pi^*$ transition of poly(acrylic acid). With the addition of APS, an adsorption over the entire UV−vis region emerges and increases with reaction time (Figure 3). A broad adsorption peak is visible at 440 nm associated with valence to anti-bipolaren transition. The adsorption reaches a maximum after a reaction time of about 2 h, followed by a decline of the absorbance across all wavelengths. The precipitation of conductive elements after a certain reaction time is possibly derived by the formation of cross-linked products. The occurrence of insoluble products after an extended reaction time is in good agreement with the conductance measurement during the course of the reaction. While the conductivity increases significantly after the initial addition of APS, an increase in resistance and therefore decrease of conductance was observed after a certain reaction time with precipitated product appearing on the electrode. (Figure 4). As a consequence, the polymerization was quenched with methanol after 1 h to prevent further oxidation and subsequent cross-linking reaction. The quenched product resulted in a black, stable solution, while the formation of precipitate was absent. A control experiment carried out in the absence of templating poly(acrylic acid) resulted in the immediate precipitation of a black product, while the aqueous solution, after filtration, was found to be only slightly colored.

The reaction was carried out with a range of ammonium persulfate concentrations starting with a concentration of $^1/_{10}$ up to $^1/_{4.5}$ of pyrrole concentration. The ratio between oxidant and pyrrole can play a crucial role, since it has been reported that a low oxidant concentration would result in incomplete oxidation with a reduced amount of polaron structures, thus lower conductivity. A high concentration of oxidant on the other hand can allegedly result in the formation of cross-linked products by additional 2,3-coupling.[36] The APS concentrations employed all resulted in the formation of products soluble in aqueous solution after quenching with methanol after 1 h reaction time. No clear correlation between solubility and APS concentration was observed. The solutions could be distinguished by the increasing UV−vis adsorption with increasing APS concentration, and a 50% increase in absorbance from the lowest to the highest APS concentration were observed. The absorbance can be directly correlated to the conductance of the solution showing that a higher oxidant concentration indeed leads to a higher conductivity due to the formation of better conjugation.[36] The correlation between oxidant and conductance has been studied in detail elsewhere,[36] while our focus in this publication is the synthesis of soluble products, which can undergo further processing.

Polymerization of Pyrrole on Self-Organized PS-*b*-PAA. The polymerization of pyrrole templated on polymers or other low molecular weight polymers is usually carried out in aqueous solution, but also in acetonitrile. However, amphiphilic block copolymers show only restricted solubility in these solvents, while in good solvents such as *N*,*N*-dimethylacetamide, the oxidation of pyrrole to polypyrrole is prevented. Pyrrole is therefore adsorbed onto the block copolymer after self-organization of PS-*b*-PAA in aqueous solution (Scheme 2). The oxidative process can therefore be carried out under aqueous conditions, which have been proven to be successful. The self-assembly of amphiphilic copolymers in aqueous media can result in the generation of a multitude of aggregate species with varying morphologies. The PS-*b*-PAA system has already been investigated in detail, and it has been found that the precise morphology depends on a combination of synergistic effects including chain stretching in the core, interfacial energy between the core and the corona, and intercorona chain repulsion.[37,38] The relative block lengths of hydrophilic and lipophilic segments can significantly influence these free energy contributions, and it has been found that, in PS-*b*-PAA aqueous systems, increasing the PS segment resulted in an increased core volume and hence larger aggregate.[37] In contrast, when the block length of PAA segment was increased, interchain repulsions between shell forming chains were augmented, resulting in an increase in surface curvature and thus a decrease in the size of the aggregate species formed. This behavior was also confirmed in our lab (results not shown here) with the aggregates typically decreasing in size with increasing size of the hydrophilic block. Typically,

Scheme 2: Schematic Drawing of Self-Assembled PS-*b*-PAA into a Micellar Structure in Aqueous Solution Followed by the Oxidation of Adsorbed Pyrrole to Polypyrrole Accompanied by a Change in Diameter of the Micelle

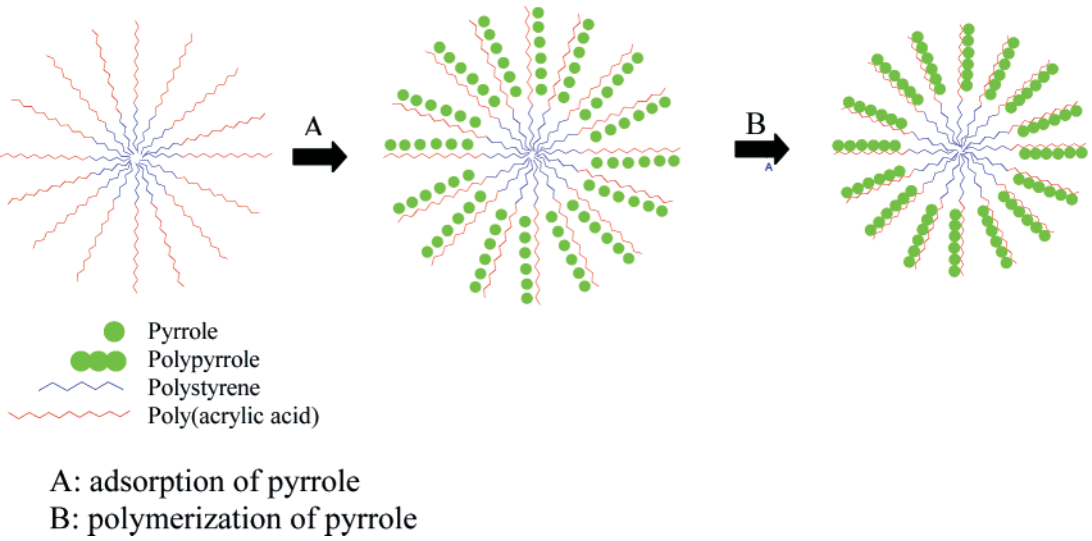

when the PAA block was increased, a transition from vesicles to rods to spheres was observed. These findings confirm an earlier detailed report by Eisenberg et al.[37,38] Analogous to these reports, we observed the formation of aggregates ranging between 80 and 200 nm in aqueous solution using DLS with a small fraction (<20%) of particles having sizes exceeding 300 nm (Figure 5a). TEM studies confirmed the formation of micelles. Figure 6 shows a typical TEM photo of the particle obtained confirming the presence of micelles. The self-assembled block copolymer in water is then treated with stoichiometric amounts of pyrrole to acrylic acid units. Significant changes of the hydrodynamic diameter with the addition of pyrrole were usually not observed despite the adsorption of pyrrole via hydrogen bonding (Figure 5b).

Upon oxidative polymerization of pyrrole, the hydrodynamic diameter of the aggregate species initially decreases quite substantially, as evidenced when APS was added to aqueous solutions of PS_{240}-*b*-PAA_{202}/Py (Figure 5c). The change in hydrodynamic diameter is equivalent to previous findings, which suggests a transition of stretched to folded poly(acrylic acid) chains.[39] The oxidation reaction was monitored in situ, by changes in D_h using PS_{240}-*b*-PAA_{200}/Py or PS_{240}-*b*-PAA_{175}/Py (Figure 7). The self-aggregate templated with pyrrole was observed to decrease in size with increasing poly(acrylic acid) length. With the addition of persulfate, a dramatic decline in D_h upon polymerizaton of adsorbed pyrrole monomer indicates that the poly(acrylic acid) corona of the micelle becomes constricted by the parallel concatenation of pyrrole. Thus, the

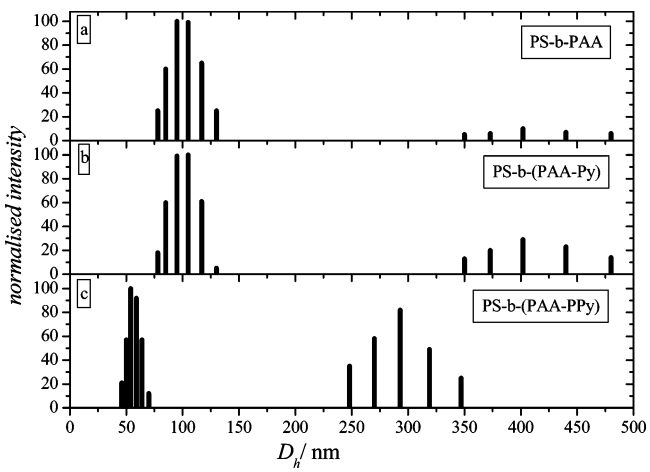

Figure 5. Particle size distribution as obtained with dynamic light scattering of aqueous solutions (1 mg mL^{-1}) of $PS_{240}-PAA_{200}$ (a) and the complexation with pyrrole to PS−(PAA−Py) (b) and the oxidation to polypyrrole PS−(PAA−PPy) (c).

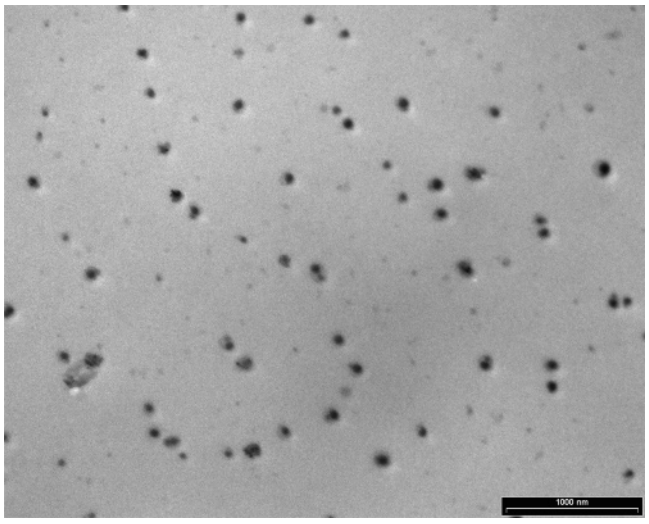

Figure 6. TEM photo of $PS_{240}-(PAA-PPy)_{200}$ obtained from an aqueous solution.

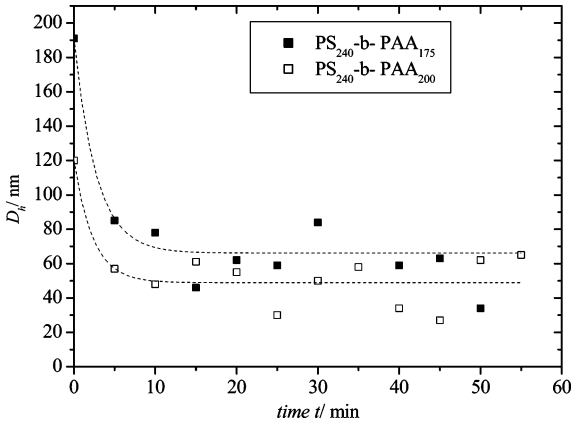

Figure 7. Hydrodynamic diameter (D_h) vs time for the polymerization of pyrrole on PS-*b*-PAA spherical micelles in aqueous solution (2.5 g L^{-1}) ([PS_{240}-*b*-PAA_{200}] = 6.38 × 10^{-5} mol L^{-1}, [Py] = 0.0197 mol L^{-1}, and [APS] = 9.90 × 10^{-4} mol L^{-1}).

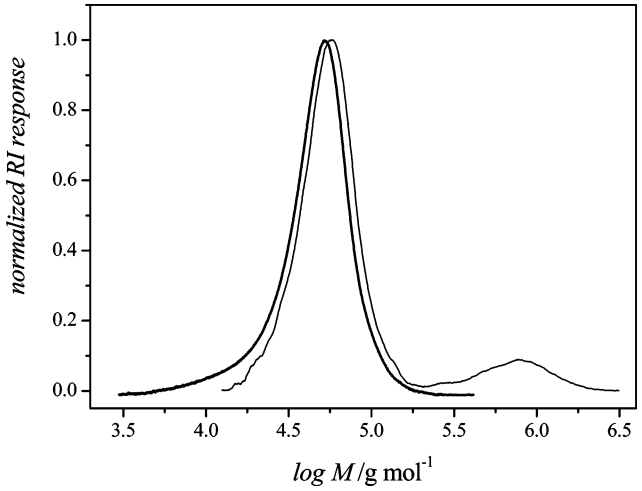

Figure 8. SEC curve in *N,N*-dimethylacetamide of PS-*b*-PAA (bold line) and the corresponding polypyrrole-based block copolymer PS-*b*-(PAA−PPy).

conformation of the outer shell changes from one which is relatively protracted and mobile to one which is quite folded and constrained due to retractile forces incurred as a result of the formation of new C−C bonds between pyrrole units. Following the initial decline in D_h, stable conformations were reached, with mean diameters on the order of 50−60 nm. The fast reduction of the diameter within the first 5 min is indicative of rapid polymerization, confirming the results obtained with conductance and UV spectroscopic measurements (Figure 3). The significant scattering of the measured diameter is due to the restricted measuring time of 2 min for each time interval. While only the diameter of the smaller particle size is displayed in Figure 7, a fraction of bigger aggregates is still present and increases slightly in percentage (Figure 5c). However, it should be noted that the scattering intensity is dependent on the particle size; hence, Figure 5 overemphasizes the real amount of the second population.

After purification using dialysis and a freeze-drying step, the product obtained was a black solid with good solubility in a range of organic solvents including chlorinated solvents, tetrahydrofuran, and *N,N*-dimethylacetamide. The SEC curves of the product show a slight shift in molecular weight of the product compared to the block copolymer used with the molecular weight increasing $M_n = 42\,000$ g mol^{-1} upon adsorption of polypyrrole (Figure 8). This molecular weight increase of 7000 g mol^{-1} corresponds to the amount of polypyrrole that is now attached to the original block copolymer. A small high molecular weight peak appears in the final conducting product, indicative of either some intermolecular cross-linking during the pyrrole oxidation or the formation of strong aggregates in organic solvents.

The sizes of these inverse aggregates in organic solvents were investigated by employing light scattering studies (Figure 9). While PS-*b*-PAA block copolymers show typical broad distributions in methylene chloride with an average diameter varying slightly with the block size (70−170 nm), the block copolymers carrying polypyrrole display in all cases extremely narrowly distributed aggregates having diameters of two to three times the size of the original inverse structure. Additionally, the typical increase in adsorption with the formation of polypyrrole over the whole wavelength range in methylene chloride solution can again be considered an indication for a conjugated system (Figure 10).

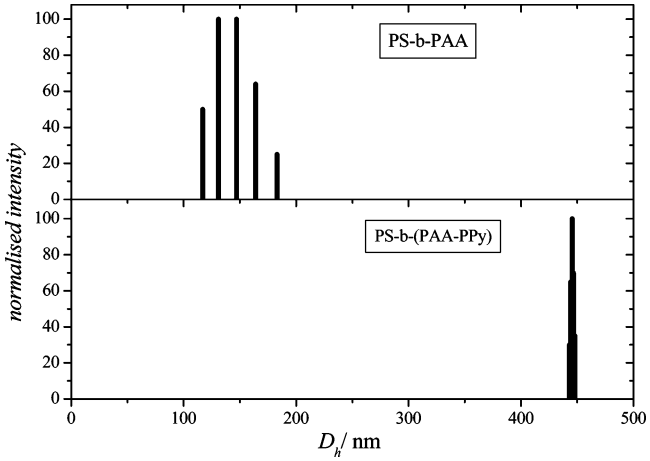

Figure 9. Hydrodynamic diameter D_h in methylene chloride of PS_{440}-*b*-PAA_{300} and the corresponding polypyrrole-based block copolymer PS_{440}-*b*-$(PAA-PPy)_{300}$ ($c = 0.5$ mg mL^{-1}).

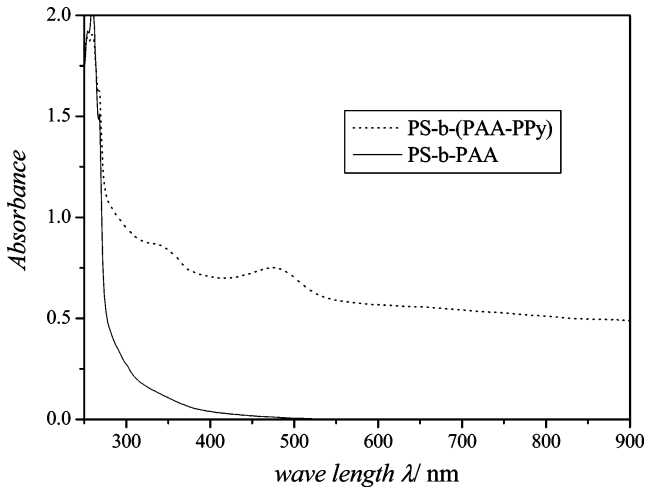

Figure 10. UV spectra in methylene chloride of PS_{440}-*b*-PAA_{300} and the corresponding polypyrrole-based block copolymer PS_{440}-*b*-$(PAA-PPy)_{300}$ ($c = 0.5$ mg mL^{-1}).

In summary, conducting polymers showing good solubility in a range of solvents ranging from halogenated solvents to aqueous solutions were prepared by a templating technique, while insoluble byproducts seemed to be either absent or restricted. The good solubility now allows the versatile processing into self-organizing structures.

Thermal Analysis. Further indication for the successful complexation of polypyrrole onto poly(acrylic acid) might be derived from the altered thermal behavior of these polymers.

DSC analyses of both homopolymer species, polystyrene and poly(acrylic acid), show a glass transition endotherm close to the expected values for PAA_{390}, while for PS_{240}, a slightly lower than expected glass transition temperature of 77 °C was recorded (sample 2, Table 1). Since the glass transition temperature is molecular-weight-dependent, a theoretical molecular weight for polystyrene can be calculated using

$$T_g = T_g^{\infty} - \frac{2 \times 10^5}{\overline{M}_n}$$

with T_g^{∞} being the glass transition temperature at infinite molecular weight. The glass transition temperature for PS with a molecular weight of 25 000 g·mol^{-1} is approximately 92 °C, which is significantly higher than that obtained, suggesting that the RAFT acid endgroup may play a role in enhancing chain

Table 1: Glass Transition Temperatures Measured at a Heating Rate of 30 K min^{-1}

sample	sample number	T_g/°C
PAA_{390}	1	102 (106)[a]
PS_{240}	2	77 (100)
PS_{240}-*b*-PAA_{230}	3	75 (100)
		110 (106)
PPy	4	(165)
PAA_{390}−PPy	5	132
PS_{240}-*b*-(PAA-PPy)$_{230}$	6	99
		135

[a] Values in brackets correspond to literature values as reported in ref 40.

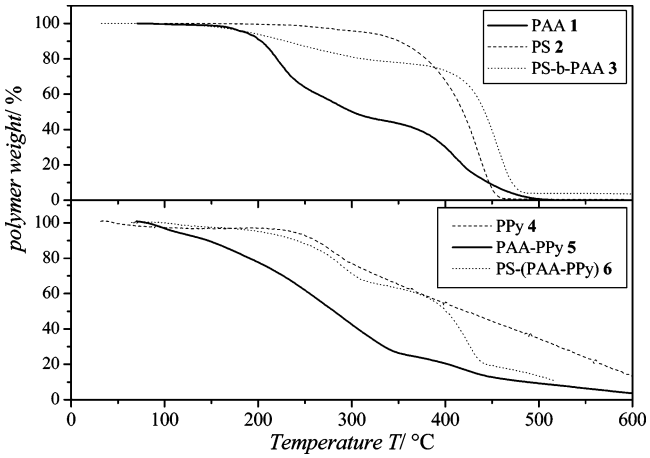

Figure 11. Thermal decomposition temperatures for homo- and diblock polymers and complexes. The numbers correspond to the samples in Table 1.

end mobility, thus lowering the observed T_g. When PS was chain extended with PAA, the glass transition temperature of PS changed very little, as expected for the generation of an amphiphilic block copolymer. Both glass transition temperatures indicate the complete phase separation as expected for incompatible blocks. However, when PAA was used as a dopant in the polymerization of Py (sample 5, Table 1), a glass transition temperature of 132 °C was observed, which is almost precisely between those for PAA (106 °C) and PPy (165 °C) (literature value[40]). This result seems indicative of some type of strong coordination between acid groups and PPy substituents, resulting in miscible polymeric chains bound by strong electrostatic forces behaving as a single species, thus exhibiting a single T_g between that of the two homopolymers. When the block copolymer species, PS_{240}-*b*-PAA_{230}, was used as a template for the oxidative polymerization of pyrrole, a complex system was formed, as indicated by the significant rise in T_g of PS by ∼22 °C from 77 to 99 °C (samples 3 and 6 in Table 1), associated with the stiffening and reinforcement of PAA blocks via coordination with PPy, thus greatly limiting chain flexibility of the block segment and the copolymer itself. The glass transition temperature for the PAA−PPy block remains unaffected, indicating the phase separation of the polystyrene block and the PAA−PPy segment.

The polystyrene macroRAFT agent exhibited a single well-defined decomposition curve at ∼386 °C, associated with chain fragmentation and generation of monomer, dimer, trimer, and tetramer species, as well as small amounts of toluene and carbon monoxide (Figure 11).[40] When chain-extended with poly(acrylic acid), the decomposition temperature of polystyrene rose significantly to ∼425 °C, denoting improved stability, possibly as a result of the replacement of the thiocarbonyl thio endgroup by the poly(acrylic acid) block. A similar trend was also observed for PAA, which exhibited both primary and secondary decomposition curves at ∼190 and ∼385 °C, related to the formation of chain fragments from monomers to octomers and small gaseous molecules, such as CO_x, H_2O, CH_4, alkenes, and ketones, respectively. When copolymerized with PS, primary and secondary decomposition curves for PAA were shifted to slightly higher temperatures, with the secondary curve overlaying that of PS at ∼425 °C (as determined by the reduction in weight percent and relative block ratios of the copolymer substitutents).

Conductive polypyrrole was found to decompose at approximately 240 °C, which is slightly lower than pristine polypyrrole, which has been reported in the range 280−300 °C[40] (Figure 11). This discrepancy may possibly be due to the presence of polaron and bipolaron structures, which may have a net destabilizing effect. When PAA^- was used as the dopant, a broad decline in weight percent was observed within the span of approximately 60−330 °C, encompassing the primary decompositions of both PPy and PAA, respectively. The complex of the block copolymer with polypyrrole exhibited two thermal decomposition peaks at ∼242 and ∼390 °C, resembling a superposition of respective component profiles. It appears that the complexation has a negative effect on the stability of the block copolymer.

Self-Organization into Honeycomb-Structured Porous Films. When certain polymers are cast from a highly volatile solvent, such as carbon disulfide (CS_2), chloroform (CH_3Cl), or benzene, the solvent quickly vaporizes, resulting in rapid cooling of the polymer solution.[16,17,41] Under humid conditions, water droplets condense onto the cold polymer solution, and since the subphase of the solvent is mobile, the droplets can assemble into a close packing arrangement to form stable, regular, hexagonal arrays, so-called breath figures.[42] The polymer precipitates from solution at the interface of these assembled water droplets, creating a solid polymer layer which ultimately encapsulates the isolated water droplets.[41] A descriptive scheme of this process is available elsewhere.[16] A range of polymers have been reported to form honeycomb-structured porous films,[16] but it is still not known what the prerequisites for the successful film formations are.[33] Regular arrays have been prepared using light-emitting,[43] semiconducting,[10] or biocompatible[44] polymers. Even highly stable films prepared from polyimides[45] or films with incorporated CdSe nanoparticles[46] were obtained. Honeycomb-structured porous films are also known to show interesting properties such as the lotus effect.[47] This bottom-up approach to the synthesis of regular porous films can be advantageous over top-down techniques such as lithography because of reduced costs. Furthermore, the versatility of this process allows the preparation of films with a range of pore sizes.[16]

The application of these films as a scaffold for cell growth has been tested using cardiac myocytes[45] and other cells.[48−50] Honeycomb-structured porous film can be considered a suitable tool to study the effect of surface and pore size on the attachment of cells because of the narrow pore size distribution.

The block copolymer PS-*b*-(PAA−PPy) is an amphiphilic block copolymer with the polypyrrole-templated poly(acrylic acid) block showing good solubility in water. We expect therefore the formation of inverse aggregates with a polypyrrole core, as discussed above. During the casting process, the amphiphilic block copolymer can either rearrange around the water droplets or solubilize water in the core of the inverse

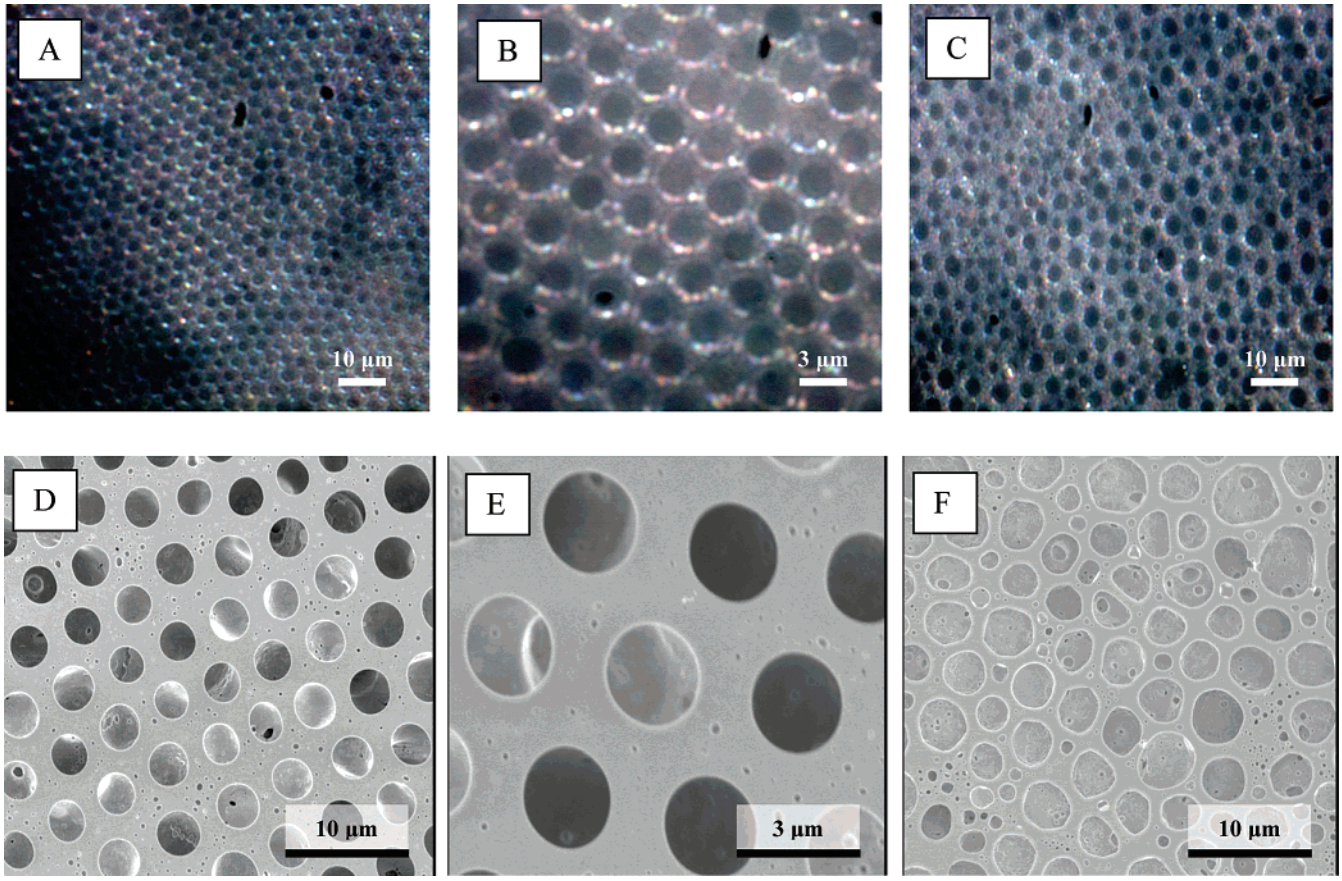

Figure 12. Optical micrographs of (A,B) PS_{240}-*b*-$P(AA-PPy)_{200}$ and (C) $PS_{440}-P(AA-Py)_{300}$, and scanning electron micrographs of (D,E) PS_{240}-*b*-$P(AA-PPy)_{200}$ and (F) $PS_{440}-P(AA-Py)_{300}$ of honeycomb-structured porous films.

structure. It was confirmed in earlier studies that the polymer interacts with the water droplet during the casting process, forming films with suborder meaning an enriched amount of hydrophilic groups within the pores.[51,52] However, this interaction prevents the essential precipitation of the polymer around the water droplet; hence, the encapsulating polymer layer is diminished. When casting PS-*b*-(PAA−PPy) a decreased regularity of the porous array with increasing hydrophilic block size was observed (Figure 12). Increasing hydrophilic block sizes delay the precipitation, confirming results obtained earlier.[51] A detailed analysis of honeycomb structures reveals that small pores ranging in the nanosize appear next to micron-sized pores, probably due to the formation of water-swollen inverse aggregates. A detailed investigation of the correlation between the block size of the amphiphilic block copolymer and the casting outcome such as pore size, regularity, and substructure is the subject of a forthcoming paper. Casting conditions were found to have a profound influence on the final result. Methylene chloride as solvent did not lead to films with any regularity. Even variations in concentration of the casting solution did not improve the outcome substantially. Carbon disulfide was found to be the better choice with concentration of the casting solution of 10 g L^{-1} resulting in regular films as long as the block copolymer is composed of a polystyrene block bigger than the hydrophilic block (Figure 12).

Cytotoxicity. Cell growth inhibition data (Figure 13) on the cytotoxicity test of various block copolymer PS-*b*-(PAA−PPy) with varying PAA−PPy sizes, at a level of 30% inhibition compared to tissue culture polystyrene controls, indicate that only 34W exhibited an inhibitory response greater than 30%, while 36W fell close to the 30% threshold. The samples cast on polypropylene disks all seem to encounter slightly higher

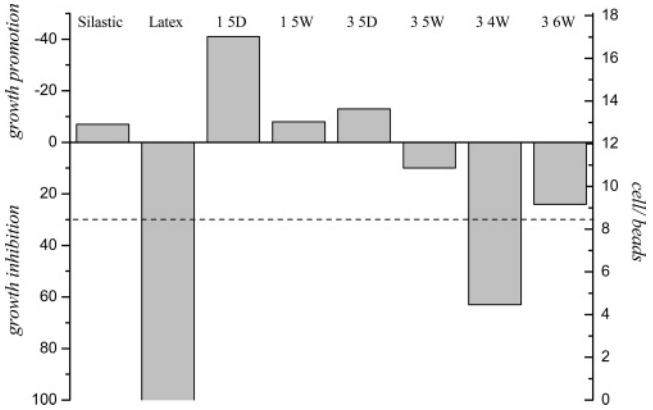

Figure 13. Cell growth inhibition of fibroblast cells on honeycomb-structured porous films prepared from $PS_{440}-P(AA-Py)_{300}$ (15), $PS_{240}-P(AA-Py)_{175}$ (34), $PS_{240}-P(AA-Py)_{230}$ (35), and $PS_{240}-P(AA-Py)_{200}$ (36) cast on glass Petri dish (D) or polypropylene disk (W).

cytotoxicity than the samples cast on a glass Petri dish. A likely reason might be the leaching of some toxic additives from the polypropylene material. All other samples exhibited little or no inhibition of cell growth, indicating that block copolymer PS-*b*-(PAA−PPy) is reasonably non-cytotoxic and biocompatible for cell culture.

Cell Attachment and Cell Growth. Attachment and growth of cells on two PS-*b*-(PAA−PPy) porous films prepared from two different block copolymers (PS_{440}-*b*-$(PAA-PPy)_{65}$, PS_{240}-*b*-$(PAA-PPy)_{230}$), in comparison to a flat-bottomed PS tissue culture well and a PS-*b*-PPy thin nonporous film, were investigated. It was found that both honeycomb-structured

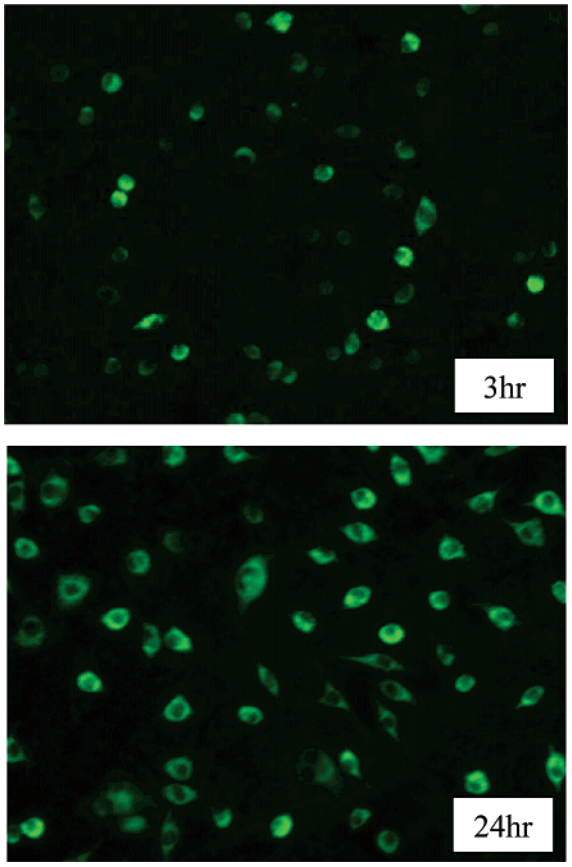

Figure 14. Fibroblast attachment on honeycomb-structured porous films, PS_{440}-*b*-$P(AA-PPy)_{65}$ with pore sizes between 1 and 2 μm after 3 and 24 h.

Table 2: Attached Fibroblast Cells L929 on a Polystyrene Dish, on a Flat Nonporous Film, and on Honeycomb-Structured Porous Films with Different Pore Sizes

sample	structure	3 h (cell/cm^2)	24 h (cell/cm^2)	growth (*X*)
PS	flat film	9800	24 400	3
PS_{440}-*b*-$(PAA-PPy)_{65}$	flat film	0	0	0
PS_{440}-*b*-$(PAA-PPy)_{65}$	pores > 1 μm	4333	4800	1.108
PS_{240}-*b*-$(PAA-PPy)_{230}$	pores < 1 μm	4433	12 100	2.729

porous films attach cells equally well at approximately 45% of the PS culture well, while no attachment was found on flat PS-*b*-PPy film (Table 2). It is believed that an increase in surface area of substrate, regardless of pore size, via a honeycomb-structured surface polymer films, assist and enhance cell contact, improving adhesion of cells onto the polymer substrate. Cell growth after 24 h on a film prepared from PS_{240}-*b*-$(PAA-PPy)_{230}$ with a pore size smaller than 1 μm was found to increase comparably (2.7×) to a flat-bottomed PS tissue cul ture well, (Table 2, Figure 15), while PS_{450}-*b*-$(PAA-PPy)_{65}$ with a lesser PPy block ratio and larger pores (>1 μm) was found to proliferate insignificantly (1.1×) (Table 2, Figure 14). These indicate that, although both block polymers have similar cell attachment characteristics, proliferation of cells are however superior when the block ratios are approximately equal and in smaller pores of honeycomb-structured porous films.

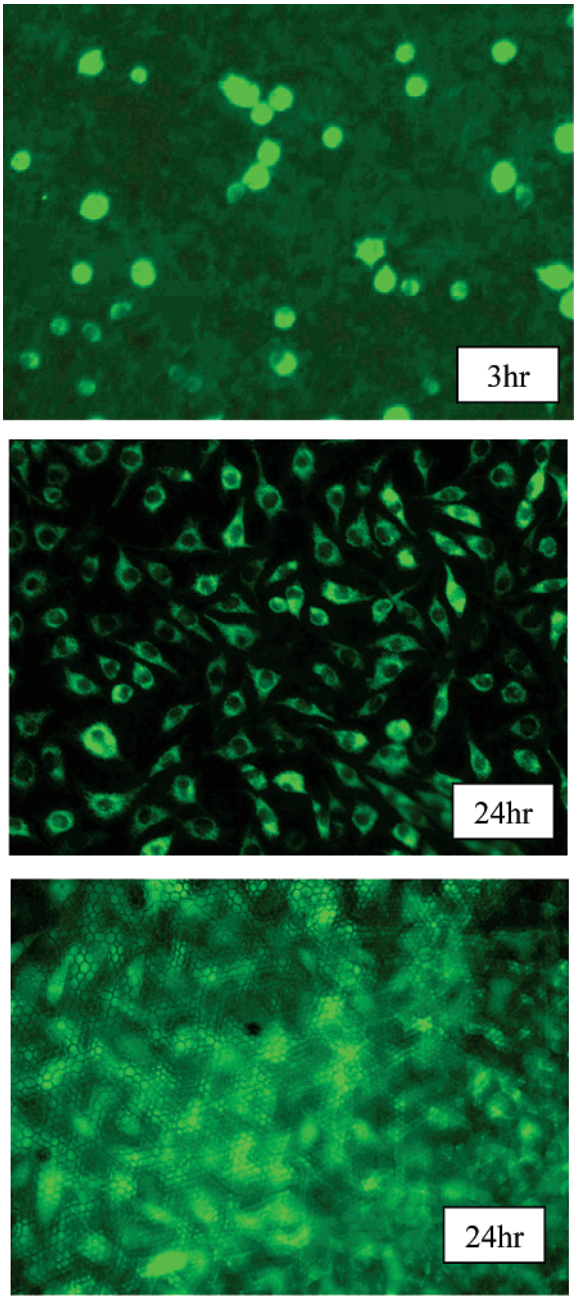

Figure 15. Fibroblast attachment on honeycomb-structured porous films, PS_{240}-*b*-$P(AA-PPy)_{230}$ with pore sizes below 1 μm after 3 and 24 h. The lower picture shows the honeycomb-structured porous films as well as the attached cells.

Conclusion

RAFT polymerization was found to be a versatile technique to generate polystyrene−poly(acrylic acid) block copolymers with a range of block sizes. The resulting amphiphilic block copolymers undergo self-organization in water leading to micellar structures. Pyrrole was templated along the poly(acrylic acid) block. The subsequent oxidation to polypyrrole resulted in the formation of conducting aggregates, which show good solubility in water as well as in organic solvent. The polymers can therefore be processed into honeycomb-structured porous films. Prior to the investigation of these films as a scaffold for cell growth, the polymer was tested regarding its toxicity showing that the cell-growth inhibition is negligible. The porosity of these films was shown to influence the cell

attachment and growth of fibroblast cells. Smaller pore sizes were observed to enhance cell attachment.

Acknowledgment. The authors would like to thank the Engineering Faculty (University of New South Wales) for financial support of this project. T.P.D. acknowledges a federation fellowship. We also would like to acknowledge the excellent management of the research centre (CAMD) by Dr. Leonie Barner and Mr. Istvan Jacenjik.

References and Notes

(1) Wallace, G. G.; Kane-Maguire, L. A. P. *Adv. Mater.* **2002**, *14*, 953.
(2) Robinson, J. F., Mark, H. B., Eds. *Conducting Polymers and Polymer Electrolytes from Biology to Photovoltaics*; ACS Symposium Series 832; The American Chemical Society: Washington, DC, 2003; pp 154−165.
(3) Collier, J. H.; Camp, J. P.; Hudson, T. W.; Schmidt C. E. *J. Biomed. Mater. Res.* **2001**, *50*, 574.
(4) Kotwal, A.; Schmidt, C. E. *Biomaterials* **2001**, *22*, 1055.
(5) Lee, J. H.; Jung, H. W.; Kang, I.; Lee, H. B. *Biomaterials* **1994**, *15*, 705.
(6) Dalby, M. J.; Riehle, M. O.; Yarwood, S. J.; Wilkinson, C. D. W.; Curtis, A. S. G. *Exp. Cell Res.* **2003**, *284*, 274.
(7) Skotheim, T. A., Elsenbaumer, R. L., Reynolds, J. R., Eds. *Handbook of Conducting Polymers*, 2nd ed.; Marcel Dekker, Inc.: New York, 1998.
(8) Joo, J.; Lee, J. K.; Hong, J. K.; Baek, J. S.; Lee, W. P.; Epstein, A. J.; Jang, K. S.; Suh, J. S.; Oh, E. J. *Macromolecules* **1998**, *31*, 479.
(9) Shen, Y.; Wan, M. *J. Polym. Sci., Part A: Polym. Chem.* **1997**, *35*, 3689.
(10) Song, K. T.; Lee, J. Y.; Kim, H. D.; Kim, S. Y.; Kim, C. Y. *Synth. Met.* **2000**, *110*, 57−63.
(11) Bhattacharya, A.; De, A.; Das, S. *Polymer* **1996**, *37*, 4375.
(12) Wang, J.; Ge, D.; Wang S. *Chem. Lett.* **2003**, *32*, 528.
(13) Pringle, J. M.; Efthimiadis, J.; Howlett, P. C.; Efthimiadis, J.; MacFarlane, D. R.; Chaplin, A. B.; Hall, S. B.; Officer, D. L.; Wallace, G. G.; Forsyth, M. *Polymer* **2004**, *45*, 1447.
(14) Malinauskas, A. *Polymer* **2001**, *42*, 3597.
(15) Wallace, G. G.; Spinks, G. M.; Kane-Maguire, L. A. P.; Teasdale, P. R. *Conductive Electroactive Polymers Intelligent Materials Systems*, 2nd ed.; CRC Press LLC: Boca Raton, FL, 2003; pp 51−119.
(16) Stenzel, M. H. *Aust. J. Chem.* **2002**, *55*, 239.
(17) Widawski, G.; Rawieso, M.; François, B. *Nature (London)* **1994**, *369*, 397.
(18) Song, L.; Bly, R. K.; Wilson, J. N.; Bakbak, S.; Park, J. O.; Srinivasarao, M.; Bunz, U. H. F. *Adv. Mater.* **2004**, *16*, 115.
(19) Le, T. P.; Moad, G.; Rizzardo, E.; Thang, S. H. International Patent PCT WO 9801478; 1998.
(20) Barner-Kowollik, C.; Davis, T. P.; Heuts, J. P. A.; Stenzel, M. H.; Vana, P.; Whittaker, M. *J. Polym. Sci., Part A: Polym. Chem.* **2003**, *41*, 365.
(21) Perrier, S.; Takolpuckdee, P. *J. Polym. Sci., Part A: Polym. Chem.* **2005**, *43*, 5347.
(22) Hales, M.; Barner-Kowollik, C.; Davis, T. P.; Stenzel, M. H. *Langmuir* **2004**, *20*, 10809.
(23) Arotcarena, M.; Heise, B.; Ishaya, S.; Laschewsky, A. *J. Am. Chem. Soc.* **2000**, *124*, 3787.
(24) Stenzel, M. H.; Barner-Kowollik, C.; Davis, T. P.; Dalton, H. M. *Macromol. Biosci.* **2004**, *4*, 445.
(25) Sumerlin, B. S.; Lowe, A. B.; Thomas, D. B.; McCormick, C. L *Macromolecules* **2003**, *36*, 5982.
(26) Loiseau, J.; Dörr, N.; Suau, J. M.; Egraz, J. B.; Llauro, M. F.; Ladaviere, C.; Claverie, J. P. *Macromolecules* **2003**, *36*, 3066.
(27) Chiefari, J.; Chong, Y. K.; Ercole, F.; Krstina, J.; Jeffery, J.; Lee, T. P. T.; Mayadunne, R. T. A.; Meijs, G. F.; Moad, C. L.; Moad, G.; Rizzardo, E.; Thang, S. T. *Macromolecules* **1998**, *31*, 5559.
(28) Ladaviere, C.; Dörr, N.; Claverie, J. P. *Macromolecules* **2001**, *34*, 5370.
(29) Stenzel, M. H.; Davis, T. P.; Fane A. G. *J. Mater. Chem.* **2003**, *13*, 2090.
(30) Wong, K. H.; Hernández-Guerrero, M.; Granville, A. M.; Davis, T. P.; Barner-Kowollik, C.; Stenzel, M. H. *J. Porous Mater.* In press.
(31) Stenzel, M. H.; Davis, T. P. *J. Polym. Sci., Part A: Polym. Chem.* **2002**, *40*, 4498.
(32) Charton, N.; Feldermann, A.; Theis, A.; Stenzel, M. H.; Davis, T. P.; Barner-Kowollik, C. *J. Polym. Sci., Part A: Polym. Chem.* **2004**, *42*, 5170.
(33) Hernández-Guerrero, M.; Barner-Kowollik, C.; Davis, T. P.; Stenzel, M. H. *Eur. Polym. J.* **2005**, *41*, 2264.
(34) Joo, J.; Lee, J. K.; Baek, J. S.; Kim, K. H.; Oh, E. J.; Epstein, W. J. *Synth. Met.* **2001**, *117*, 45.
(35) Shen, Y.; Wan, M. *J. Polym. Sci., Part A: Polym. Chem.* **1997**, *35*, 3689.
(36) Song, M. K.; Kim, Y. T.; Kim, B. S.; Kim, J.; Char, K.; Rhee H. W. *Synth. Met.* **2004**, *141*, 315.
(37) Zhang, L.; Eisenberg, A. *Macromolecules* **1999**, *32*, 2239.
(38) Terreau, O.; Bartels C.; Eisenberg, A. *Langmuir* **2004**, *20*, 637.
(39) Zhang, W.; Shi, L.; An, Y.; Wu, L.; Gao, L.; Liu, Z.; Ma, R.; Meng, Q.; Zhao, C.; He, B. *Macromolecules* **2004**, *37*, 2924.
(40) Brandrup, J.; Innergut, E. M.; Grulke, E. A. *Polymer Handbook*, 4th ed.; Wiley Interscience: New York, 1999.
(41) Karthaus, O.; Maruyama, N.; Cieren, X.; Shimomura, M.; Hasegawa, H.; Hashimoto, T. *Langmuir* **2000**, *16*, 6071
(42) Lord Rayleigh *Nature (London)* **1911**, *86*, 416.
(43) Barner-Kowollik, C.; Dalton, H.; Davis T. P.; Stenzel, M. H. *Angew. Chem., Int. Ed.* **2003**, *42*, 3664.
(44) Nishikawa, T.; Nonomura, M.; Arai, K.; Hayashi, J.; Sawadaishi, T.; Nishiura, Y.; Hara, M.; Shimomura, M. *Langmuir* **2003**, *19*, 6193.
(45) Yabu, H.; Tanaka, M.; Ijiro, K.; Shimomura, M. *Langmuir* **2003**, *19*, 6297.
(46) Böker, A.; Lin, Y.; Chiapperini, K.; Horowitz, R.; Thompson, M.; Carreon, V.; Xu, T.; Abetz, C.; Skaff, H.; Dinsmore, A. D.; Emrick, T.; Russell, T. P. *Nat. Mater.* **2004**, *3*, 302.
(47) Yabu, H.; Shimomura, M. *Langmuir* **2005**, *21*, 3235.
(48) Haris, P. I.; Tanaka, M.; Takebayashi, M.; Miyama, M.; Nishida, J.; Shimomura, M. *Biomed. Mater. Eng.* **2004**, *14*, 439.
(49) Nishida, J.; Nishikawa, K.; Nishimura, S.-I.; Wada, S.; Karino, T.; Nishikawa, T.; Ijiro, K.; Shimomura, M. *Polym. J.* **2002**, *34*, 166.
(50) Nishikawa, T.; Nishida, J.; Ookura, R.; Nishimura, S.-I.; Wada, S.; Karino, T.; Shimomura, M. *Mater. Sci. Eng.* **1999**, *8*−*9*, 495.
(51) Stenzel, M. H.; Davis, T. P. *Aust. J. Chem.* **2003**, *56*, 1035.
(52) Nygard, A.; Barner-Kowollik, C.; Davis, T. P.; Stenzel, M. H. *Aust. J. Chem.* **2005**, *58*, 595.

BM050858M